Research Article ISSN 2771-666X

Journal of Advanced Materials Science and Engineering

Formation and Electrochemical Assessment of Flexible Supercapacitor Yarns Directly Integrated into Woven Structures

Bansari Joshi[1], Nanfei He[2], Wei Gao[2]*, Janie Woodbridge[1] and Abdel-Fattah Seyam[1]*

[1]Department of Textile and Apparel Technology and Management, Wilson College of Textiles, North Carolina State University, Raleigh, NC 27606, USA.

[2]Department of Textile Engineering, Chemistry, and Science, Wilson College of Textiles, North Carolina State University, Raleigh, NC 27606, USA.

***Correspondence:**
Wei Gao, Department of Textile and Apparel Technology and Management, Wilson College of Textiles, North Carolina State University, Raleigh, NC 27606, USA.

Abdel-Fattah Seyam, Department of Textile and Apparel Technology and Management, Wilson College of Textiles, North Carolina State University, Raleigh, NC 27606, USA.

Received: 07 Mar 2024; **Accepted:** 11 Apr 2024; **Published:** 19 Apr 2024

Citation: Joshi B, He N, Gao W, et al. Formation and Electrochemical Assessment of Flexible Supercapacitor Yarns Directly Integrated into Woven Structures. J Adv Mater Sci Eng. 2024; 4(2): 1-12.

ABSTRACT

Yarn-shaped energy-storage devices, including supercapacitor yarns and battery yarns, have been widely reported in literature, but their seamless integration into a base textile fabric (or substrate) using automatic weaving processes is yet to be fully demonstrated and explored. Here we present a set of woven fabrics formed using an automatic weaving machine. The fabrics were carefully customized to directly integrate a set of flexible supercapacitor yarns developed in our labs into different textile base (substrate) fabric structures. Two structures were formed: single-layer plain weave and double-layer plain weave designs with carefully selected structural parameters to protect the supercapacitor yarns during weaving and end use applications. The double-layer plain weave was formed with tubes strategically placed in the fabric to accommodate the supercapacitor yarns with thought to provide them with more protection than single-layer plain weave from stress during end use. Each electrode of the supercapacitor was formed by covering carbon fiber tow(s) with two coats of Polyvinyl alcohol (PVA) based gel electrolyte and a double wrap of PVA flat multifilament yarn between the two coats as electric insulator. The electrochemical integrity of the supercapacitor yarns was not negatively affected by the rigor of weaving whether woven in warp or weft direction and endured long exposure to extreme hot/humid and cold environments, accelerated distress, and surface abrasion. The double-layer plain weave structure allowed the supercapacitor yarns to sustain a longer duration of surface abrasion as compared to the single-layer plain weave structure. This work sheds light on existing myths of electronic textiles, where electronic components and textile yarns need to be integrated in an organic manner within textile structures for wearable textiles and other smart textile products.

Keywords

Supercapacitor Yarn, E-Textiles, Wearable Textiles, Smart Textiles, Energy-storage Yarns.

Introduction

Recently smart wearable technologies/electronics such as jewelry, accessories, medical devices, and clothing or elements of clothing have advanced rapidly to improve people's lives. The most advanced commercial non-textile wearable technology examples include health monitoring devices, smart rest band for tracking children, smart watches, Artificial Intelligent (AI) hearing aid, Google Glass and Microsoft's HoloLens, and a holographic computer in the form of a virtual reality (VR) headset. The advanced wearable technology devices can transfer data (to health care providers, security, and parents), provide feedback to users, and transfer/exchange data *via* internet of things (IoT). The energy sources for non-textile wearables include batteries, solar cells, or supercapacitors in a solid form. These power sources are currently

used in wearable textiles and other e-textiles and may cause discomfort pressure points to the wearers due to their large size and solid nature. Moreover, solid state power sources may cause stress concentration to the textile substrate and lead to premature failure of the product.

With the increase of the market share of wearable textiles in today's technical market sector, the interest for pliable power sources able to be integrated into a textile garment has thrived recently [1-3]. In addition to comfort, reliability, and safety, these power sources need to withstand a variety of use conditions including the extreme cases in athletic wear and military applications [4,5]. Along this line, electronic/wearable textiles, or even the concept of "smart textiles" have come into the play. Most of the exiting demos involve the attachment of commercial (rigid) electronic devices to an article of clothing with applications mostly in performance sports or futuristic fashion shows [6,7]. An actual smart fabric comprising the seamless integration of soft electronics within the textile itself is still mainly in the R&D stages at prohibitively high manufacturing cost, primarily due to the safety concerns and limited automation capabilities (machine-weaving/knitting as opposed to hand-weaving/knitting).

To zoom onto energy-storage yarns in particular, most reports in literature focus more on the technical aspects of these yarn-shaped batteries and supercapacitors, including the materials selection for electrodes, current collectors, electrolytes, and even separators, the device configuration engineering, and also the performance optimization, whereas their direct weaving on an automatic weaving machine is seldom demonstrated, let alone studied [8-10]. For example, Liu et al. displayed a woven fabric with supercapacitor yarns incorporated, however, the specific weaving technique and the electrochemical performance of supercapacitor yarns after weaving were missing [11]. Among the few machine-weaving related reports, Khudiyev et al. introduced their fiber supercapacitors as weft yarns into a double weave channel and demonstrated their good capacitance retention after machine weaving [12]. Recently, Peng's group also wove their fiber batteries into a fabric as weft yarns using a rapier weaving machine and later studied the battery stability against different environmental disturbances [13,14]. Although yarn-(or fiber) shaped supercapacitors and batteries have been demonstrated to be capable of being incorporated into woven fabrics *via* an automatic machine, they are simply described as weft and fabric details are lacking from a weaving perspective.

So far, the machine-weaving involved studies have all used rapier weaving machines [15]. Rapier weaving is shuttleless where the weft yarn package(s) are stationary, and each weft yarn has to be cut after each weft insertion. As a result, in the final woven fabrics, the length of each weft yarn is limited to the width of the fabric. This unavoidably limits the unit length of the supercapacitor or battery yarns involved in the weft direction, a fundamental structural feature that greatly impacts their electrochemical output. In addition, the weaving process induces a variety of mechanical disturbances on yarns, such as stretching, compression, abrasion, impact, etc., which then affects the yarn configurations in the fabric [16]. The effect of weaving conditions on the structural characteristics of yarn-shaped batteries or supercapacitors in the fabric, such as their lengths, arrangement pattern, strategic placement, etc., as well as how to adjust weaving conditions correspondingly to better accommodate and protect these functional yarns, have yet to be thoroughly explored.

In this work, we developed several flexible supercapacitor yarns and directly integrated them into base (or substrate) textile structures using automated shuttle weaving machine. The weaving process variables, weave structure, and fabric structure parameters were carefully designed to enable direct integration of yarn-shaped supercapacitors (YSCs) with desired placement in the fabric to protect them during manufacturing and end use. The performance of the YSCs in different woven configurations was evaluated. Four fabric structures containing YSCs were woven and their electrochemical performance was assessed to investigate the integrity of the YSCs upon different manufacturing scenarios. The woven fabrics containing the YSCs were then subjected to extreme environmental conditions, accelerated distress, and surface abrasion to evaluate the electrochemical performance of the YSCs in different application conditions. The following questions were taken into consideration which can impact the electrochemical performance of the YSCs:

i. How do different yarn arrangements and weave constructions affect the performance of the YSCs, such as YSC woven in warp *vs.* weft direction, single-layer fabric *vs.* tubes of double-layer fabric?
ii. Can the placement and weave structure impact the performance of the YSCs once it is in application and put under extreme weather conditions, distress, and surface abrasion?

The data collected from these weave constructions and tests will help to evaluate the factors that contribute to the performance of the YSCs in industrial production scenarios and in ultimate civilian and defense applications that are necessary for successful commercialization.

Materials and Methods

YSCs Structure and Formation

Two types of YSCs were fabricated using different electrode materials. One YSC was constructed from activated carbon (AC) coated 1k carbon tow as electrodes. The other was composed of two twisted 1k carbon tows as electrodes. The activated carbon yarn-shaped supercapacitor will be termed AC YSC throughout the paper. To differentiate, the yarn-shaped supercapacitor without AC is referred to as non-AC YSC. Figure 1a and Figure 1b show the two YSC designs with one electrode each. To form the final structures, each YSC underwent several processes to achieve the functionality of supercapacitor in a flexible textile yarn form. The YSCs were formed by applying a Polyvinyl Alcohol (PVA) based coating H_3PO_4/PVA/H_2O gel electrolyte (blue) onto electrode, double wrapping PVA (Polyvinyl Alcohol) flat multifilament yarn (green) as separators to prevent the two electrodes from contacting

each other and causing short circuits and applying additional coating of H_3PO_4/PVA/H_2O gel electrolyte [17]. To form the final AC YSC and non-AC YSC supercapacitors, two yarns of Figure 1a and Figure 1b where twisted together. Figure 1c illustrates the longitudinal cross-sectional schematics of non-AC YSC (left) and AC YSC (right) final devices with two electrodes each.

Several YSCs were formed and tested for their tensile properties (load-elongation and cyclic loading), which are related to weavability. The yarns that exhibited the best electrochemical performance and smallest diameters (highest flexibility for wearer comfort) were integrated into woven fabrics described later. The diameter of AC YSC and non-AC YSC were 1.08 mm and 1.3 mm, respectively. Details on the equipment and methods utilized to form the two YSC structures are covered elsewhere [18].

Fabric Formation

The YSCs were integrated into single-layer and double-layer plain weave fabrics (Figure 2). The base woven fabrics (substrate) were formed from a 40/2 Cotton Count (2x14.76 tex) combed, ring spun, mercerized cotton yarn as warp and a 4/8 worsted count (4x110.73 tex) weight shrink treated spun merino wool as weft yarn. The warp yarn diameter measured in both types of fabrics was 0.31 mm. The wool weft yarn diameter measured in the fabric was 1.36 mm and 1.17 mm for single-layer and double-layer fabrics, respectively, which is intentionally set to be higher than the diameter of the AC YSC, as it is essential for protecting the supercapacitor yarns from the surface abrasion and pressure loading during physical testing and end use. The difference in the wool yarn diameter in single-layer and double-layer fabrics is due to the intentional higher weft density in the double layer to substitute for the half warp in a layer as the warp density (threads/unit fabric width) for both types of fabrics is the same since one warp was used to weave the experimental fabrics. The high weft density (or tightness) in the double-layer fabric provided less room for the wool weft yarn that caused the reduction in its diameter in the fabric.

Formation and Structure of the Woven Experimental Fabrics

An automated computer controlled AVL shuttle loom equipped with a CAD driven dobby shedding system with 24 harnesses was utilized to manufacture the experimental woven fabrics containing the YSCs. The cotton warp yarn sequence was in two alternating white and black (1W, 1B sequence) colors and set in a 24-harness straight draw and on-loom warp density 33.1 threads/cm (84 threads/inch) and off-loom warp density 35 threads/cm (88.9 threads/inch) due to width shrinkage. The on-loom and off-loom, which are identical, weft density of the single-layer plain weave and double-layer plain weave fabrics were 5.67 threads/cm (14.4 threads/inch) and 17.14 threads/cm (43.56 threads/inch),

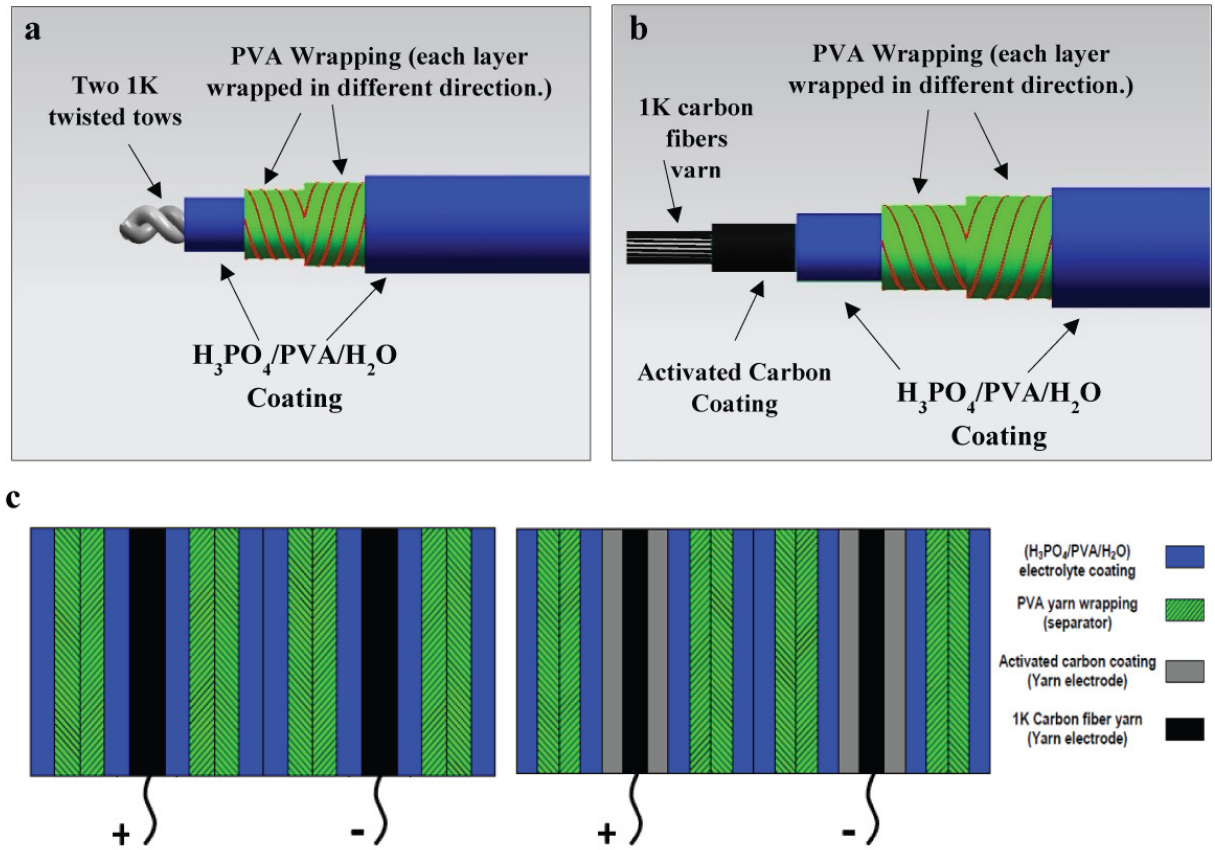

Figure 1: Structure of supercapacitor yarns. (a) Non-AC YSC's yarn electrode (b) AC YSC's yarn electrode, (c) longitudinal cross section view of the final supercapacitors.

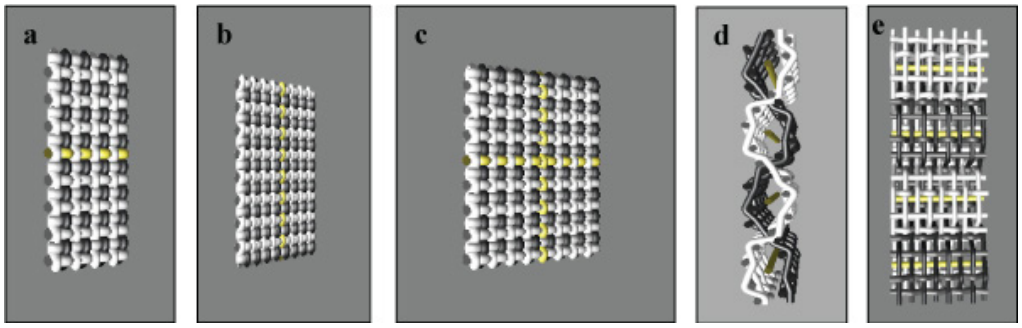

Figure 2: Experimental fabrics with YSC yarns integrated. (a) Single-layer plain weave with YSC in the weft direction (b) Single-layer plain weave with YSC in the warp direction (c) Single-layer plain weave with YSC in both warp and weft directions (d) Side view of double-layer plain weave with YSC yarn inserted in tubes in the weft direction and (e) Front or flat view of (d).

respectively. The weft density per layer in the double-layer fabric is 8.57 threads/cm (21.78 threads/inch). The warp and wool weft crimp due to weave interlacing of both types of fabrics were 31% and 2.6%, respectively. The cotton warp yarn is much thinner than the weft wool yarn and YSCs that causes the warp yarn to exhibit significantly higher crimp than the weft yarns. Due to the size and structure the YSCs' weave-induced crimp was 0% as these yarns are stiffer than the cotton warp yarns.

The AVL loom is equipped with four shuttle boxes on either side of the machine that allowed the formation of variety of weave structures with the objective of directly integrating the YSCs and the wool yarns (black and white) into woven structures in a desired sequence in the weft direction. The YSCs were wound onto pirns (weft yarn packages) and then placed into a dedicated shuttle. The white and black wool weft yarns were also wound onto pirns and placed in dedicated shuttles. After pirn winding, the shuttles were placed into the shuttle boxes of the automated AVL weaving machine. The sequence of the wool weft yarns (black and white) and YSCs was preprogrammed *via* digital shuttle selection system. As opposed to shuttleless weaving, whereas the weft yarn maximum length equals the fabric width due to cutting the weft yarn after each insertion, in shuttle weaving, weft yarn is continuous which is advantageous in weaving supercapacitors with desired length distributed along the fabric length to achieve required energy and power density required for wearable and other textile products.

Four different designs of woven fabric were developed to weave experimental samples with the YSCs directly integrated into the weave structures. Woven designs were developed using WeavePoint 8 Computer Aided Design Software that controls the dobby shedding system during weaving to weave the experimental structures. The four types of fabric developed were (refer to Figure 2):

1. Single-layer plain weave with the YSCs in weft direction (Figure 2a)
2. Single-layer plain weave with the YSCs in the warp direction (Figure 2b)
3. Single-layer plain weave with the YSCs in both warp and weft directions (Figure 2c)
4. Double-layer plain weave with tubes along weft direction for automatic placement of the YSCs inside the tubes in the weft direction (Figures 2d and 2e); each tube is formed from 4 face wool weft yarns (top layer) and 4 back wool weft yarns (bottom layer)

These specific weave constructions and yarn configurations were developed to test out the YSCs in a variety of different scenarios which would simulate the types of mechanical disturbances that the yarns experience during weaving process and wear by the end users. For reasons that will be addressed later, physical tests were conducted on AC YSCs integrated into single-layer and double-layer plain weave fabrics in the weft direction. In the single-layer fabric, the sequence of the weft yarns was three black wool yarns followed by one AC YSC. In the double-layer fabric, for a given tube, the sequence of the weft yarns (9) was: 1 B, 1 W, 1 B, 1 W, 1 AC YSC, 1 B, 1 W, 1 B, 1 W (where B is black wool yarn and W is white wool yarn). To obtain the tubular structure of Figure 2d, the black cotton warp and wool weft yarns were woven as top layer (seen as a black horizontal stripe in Figure 2e and Figure 10 right) for the sequence of the 9 weft yarns given above and white cotton warp and wool weft yarns were woven as top layer for the next 9 weft yarns (seen as white stripe in Figure 2e and Figure 10 right). The 18-yarn sequence was repeated to obtain the desired number of tubes/AC YSCs. With this structure, the double-layer fabric was intentionally designed with stitches at the interchange of the white and black warp yarns to provide tubes with a specific size to accommodate the AC YSCs in the middle of each tube. Technically, this structure is a three-layer woven fabric where the cotton and wool yarns form the top and bottom layers, and the AC YSC forms the center layer. The single-layer plain weave fabric required two shuttles; one for the black wool yarn and one for the AC YSC, while the double-layer fabric required three shuttles; one for the black wool yarn, one for the white wool yarn, and one for the AC YSC. The required sequence of the shuttles (weft yarns) and the weave structures were preprogramed using the CAD system of the AVL shuttle weaving machine.

Woven Fabric Testing

E-textiles components (electronics and substate) experience a broad range of environmental and mechanical conditions including the extreme cases of civilian and defense applications [19,20]. To evaluate the performance of the YSCs integrated in the woven fabrics, we ran different physical tests, environmental tests,

accelerated mechanical distress tests and Wyzenbeek abrasion tests. Throughout the experiment we focused on two fabric design samples: the single-layer plain weave and double-layer plain weave samples with the AC YSCs in weft direction, as shown in Figures 2a and 2d, respectively. The justification for this focus is given in the results and discussion section. Figure 2d shows that there is one AC YSC integrated in each tube, while in the single-layer plain woven samples (Figure 2a and Figure 10 left), the weft sequence was three wool yarns followed by one AC YSC.

The environmental test was used to simulate the conditions of extreme environments to test the performance limits of the AC YSCs in different climates. The fabric samples were placed in a walk-in environmental room that was adjusted to extreme heat and relative humidity (45˚C and 80% RH) and then placed in a freezer to subject them to extreme cold (-21˚C) condition.

In the absence of standard test, an accelerated mechanical distress test based on applying pressure resulting from a normal force on the experimental woven samples was thought. The accelerated mechanical distress test was used to assess certain performance stresses that applied weight could have on fabrics containing the AC YSCs. To simulate a heavy real-life ultimate stress situation, we considered the weight of a heavy backpack of 22.68 kg (50 lbs). We assumed maximum pressure on a wearable article considering the weight of the backpack and its dimension of 68.58 cm x 53.34 cm (27 inch x 21 inch). Given the weight and the dimensions of the backpack, the pressure was 606.74 Pascal (0.088 lbs/inch^2). A 2.722 kg (6 lbs) metal plate was used to distress the samples containing AC YSC of dimension of 45.72 cm x 9.525 cm (18 inch x 3.75 inch) to simulate the maximum distress that a wearable article experiences from a backpack during wear. The pressure was calculated by assuming the force from the backpack is applied in the perpendicular direction to the wearable textile article, which is much higher than the actual pressure. We assumed a backpack use of 3 hrs max every day. Each experimental sample was pressured for 3 hrs then the load was removed for 21 hrs. This was repeated for 6 days. The electrochemical properties were measured before applying the pressure and after each 3 hrs of loading for six cycles.

The abrasion test was conducted according to the ASTM D4157-13 using Wyzenbeek abrasion equipment. It was designed to examine the performance of the AC YSCs in the fabric under different harsh abrading situations to simulate what civilian and military wearable article experience during end use. #10 Cotton Duck per the test standard and 800-grit sandpaper were used as abradants against single-layer plain weave and double-layer plain weave fabrics containing the AC YSCs in the weft direction. The abrasion tests were conducted for a certain number of cycles after which the test was stopped, and the electrochemical performance of AC YSC was measured. This was repeated until the base woven fabric was torn since the AC YSC would not survive after the textile substrate failure. To ensure the abrader and a woven sample have the same contact area, electrochemical performance testing was conducted while the sample is mounted in the abrasion tester.

Result and Discussion

The following sections cover comparisons between the electrochemical performance of the non-AC YSCs and AC YSCs in different weave constructions before and post weaving process and different physical testing.

Comparison of Electrochemical Properties of Non-AC and AC YSCs

The electrochemical performance of YSCs was evaluated with cyclic voltammetry (CV) curves (Figure 3a) and Nyquist plots at 0.01 Hz to 10^6 Hz (Figure 3b). The AC YSC showed a quasi-rectangular shape of its CV curve, which was significantly larger in area than the non-AC YSC, indicating the higher capacitance due to the presence of AC, a well-accepted electrode material for commercial supercapacitors. The capacitance of non-AC YSC and AC YSC were 0.0011 mF and 3.42 mF, corresponding to specific linear capacitance of 0.0001 mF cm^{-1} and 0.342 mF cm^{-1}, respectively. The Equivalent series resistance (ESR) obtained from Nyquist plots was 45 Ω for AC YSC, slightly lower than 52 Ω for non-AC YSC. Overall, the AC YSC exhibited superior electrochemical performance compared to the non-AC YSC, with much higher capacitance and lower resistance.

The mechanical performance was evaluated by tensile testing. As shown in Figure 3c, AC YSC exhibited a peak load of 1,795.37 gf at an elongation of 10.6%. In comparison, the non-AC YSC showed a significantly higher peak load of 9,597.57 gf at 6.1% elongation, attributed to more carbon fibers in the electrode yarns (1k x 4 carbon tows for non-AC vs 1k x 2 carbon tows for AC). Cyclic tensile behavior was performed at 2% elongation over ten cycles. Both YSCs displayed permanent unrecoverable extension after the first cycle. For subsequent cycles, the load-elongation curves overlapped well, indicating the absence of permanent unrecoverable extension during repetitive stretching and recovery. Overall, the non-AC YSC demonstrated superior mechanical performance. However, the mechanical performance indicates that both YSCs can endure the complex field of stresses during weaving whether they are woven in warp or weft direction.

The influence of the Weaving Process on the Electrochemical Performance of YSCs

The electrochemical performance of the non-AC YSC woven in different constructions was characterized before and after the weaving process. These different constructions are: (1) Single-layer plain weave with non-AC YSC integrated in the base fabric in the weft direction, (2) Single-layer plain weave with non-AC YSC integrated in the warp direction, (3) Single-layer plain weave with non-AC YSC integrated in the weft and the warp directions, and (4) Double-layer plain weave with AC YSC and non-AC YSC integrated in tubes in the weft direction (refer to Figure 2).

After involved as weft yarns in single-layer plain weave, the capacitances of non-AC YSC and AC-YSC exhibit a fluctuation of less than 3%. As shown in Figure 4, while the CV and Nyquist plots of non-AC YSC exhibit significant overlap before and after weaving, AC-YSC displays a minor deviation in both CV and

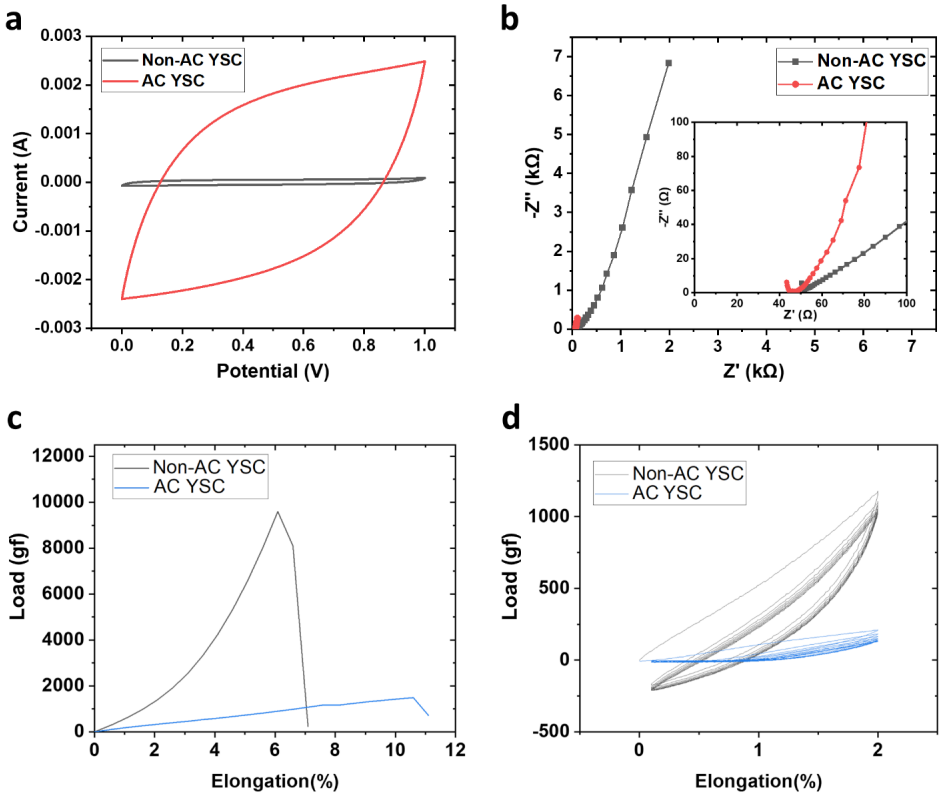

Figure 3: Electrochemical and tensile performance of Non-AC YSC and AC YSC of 10 cm long. (a) CV curves at scan rate of 40 mV s^{-1}; (b) Nyquist plots (1 M – 0.01 Hz), with the insert highlighting the high-frequency region of the plots; (c) Tensile test; (d) Cyclic tensile test.

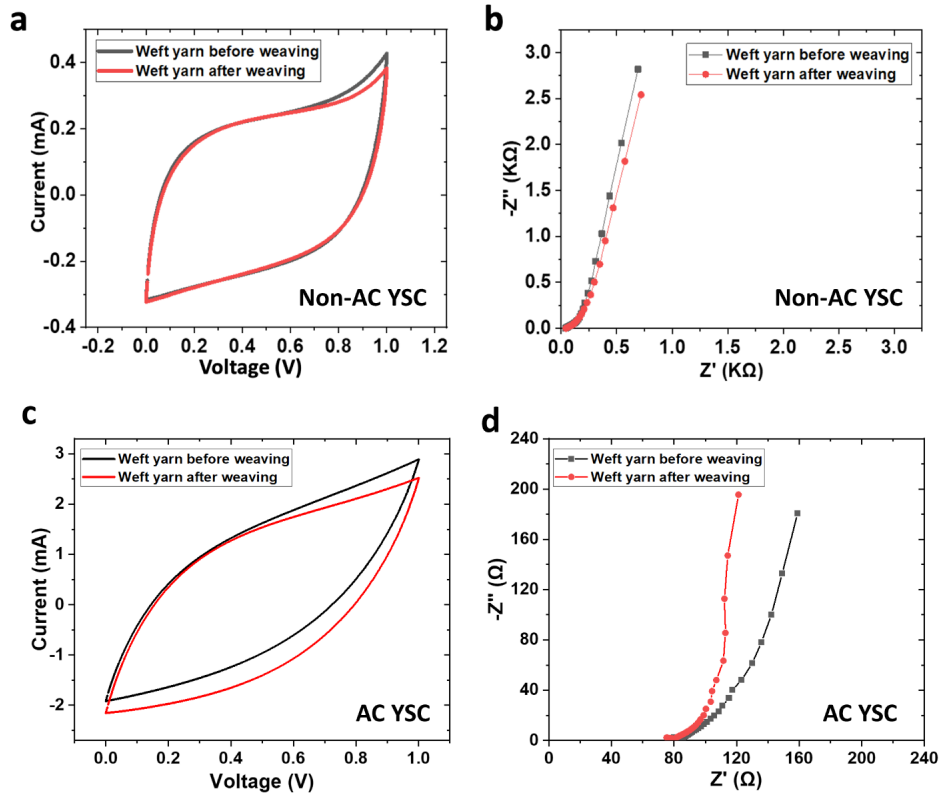

Figure 4: Electrochemical characterization of 45.72 cm long non-AC YSC and AC YSC woven in weft direction before and after weaving. (a) CV curve (40 mV s^{-1}) and (b) Nyquist plot of non-AC YSC; (c) CV curves (40 mV s^{-1}) and (d) Nyquist plot of AC YSC.

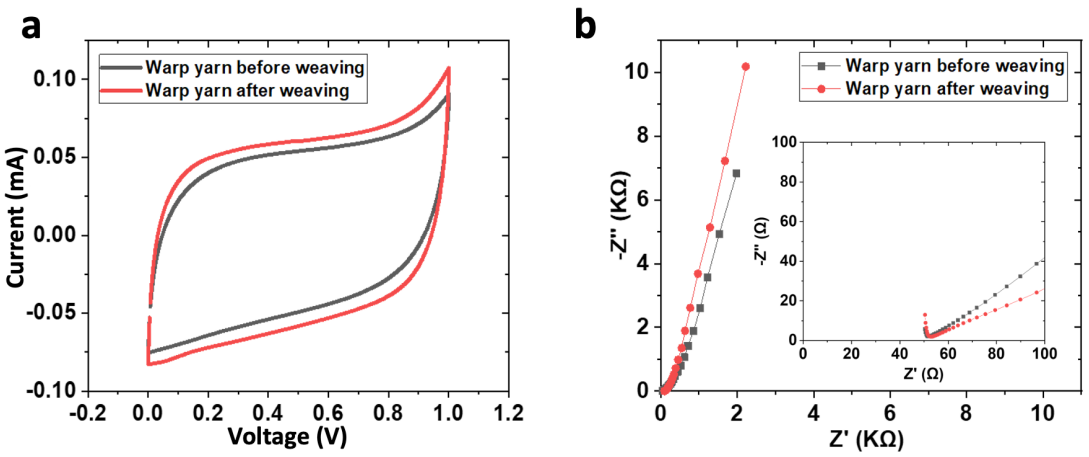

Figure 5: Electrochemical performance of 10 cm long non-AC YSC woven in warp direction before and after weaving. (a) CV curves (40 mV s^{-1}) and (b) Nyquist plot, with the insert highlighting the high-frequency region of the plots.

Nyquist plots. This divergence can be attributed to the potential influence of the weaving process on the contact between AC particles and carbon yarns, resulting in this slight performance deviation in CV. In terms of the Nyquist plot, better diffusion of electrolyte ions is evidenced by a more vertical curve in the lower-frequency domain, which is to our surprise. We suspect that the segmented compression coming from the warp yarns interlacing may be contributing to this change in the AC-YSC case, since the porous AC electrode can benefit from a localized pressure for contact improvement.

YSCs have been incorporated in both warp or weft directions, as well as in single- or double-layer plain woven fabrics. Among these different structures, YSCs that are inserted as warp yarns exhibit the most notable influence on their electrochemical performance. As shown in Figure 5a, the warp non-AC YSC in a single-layer plain weave increases by 13.86% in capacitance after weaving. The resistance of non-AC YSC remains relatively stable (Figure 5b). However, this difference is practically negligible in terms of overall performance comparison. In summary, these results reveal that there is no significant difference in the electrochemical characteristics of these YSCs before and after weaving, regardless of their direction (warp or weft), or the specific weave structure (single- or double-layer plain weave).

Physical Testing

The results of Figure 3 indicate the superior performance of AC YSCs over the non-AC YSCs and the results of Figures 4 and 5 disclosed that the electrochemical performance of YSCs in warp and weft directions were slightly affected by the weaving process stresses, perhaps due to the stress-induced contact degradation between electrodes. For these reasons, as well as the smaller diameter and higher flexibility of AC YSCs compared to the non-AC YSCs, the physical tests were conducted on AC YSCs integrated into the substrate (base fabric) in single-layer plain weave and double-layer plain weave, where tubular structures are accommodating the AC YSCs in the weft direction. As stated earlier, weaving the YSCs in weft direction in shuttle weaving provides the opportunity to weave them in continuous length along the fabric width and length, and thus design wearable textiles with desired power source depending on applications.

The Influence of Extreme Environmental Conditions on AC YSCs' Electrochemical Performance

This test was designed to subject the experimental samples to cycles of extreme hot and humid (45˚C and 80% RH) environment for 24 hrs. followed by extreme cold condition (-21 ˚ C) for 24 hrs. The 48 hrs. Cycle was repeated 3 times. The electrotechnical performance of the AC YSCs integrated in single-layer and double-layer plain weave fabrics were measured before the environmental test (control) and after each cycle. The results of the electrochemical performance are shown in Figure 6. The deviation of the "before test" CV curve from ideal rectangular shape is primarily due to the gel electrolyte we adopted for these YSCs, the H_3PO_4-PVA system, which tends to dry out quickly and gives compromised ionic conductivity. Improvements in gel electrolyte can be made to mitigate this issue, which will be discussed in our future publications.

In Figure 6a, the CV results of AC YSC constructed in single-layer plain weave after the 2nd and 3rd cycles of exposure to the extreme environment are perfectly superimposed. It can be noticed from the figure that the CV curves of the control and exposed samples after three cycles of exposure are very close with insignificant differences. The results of the resistance of AC YSC in Figure 6b are very close with insignificant difference between the 2nd and 3rd cycles, while comparing to the value before testing, a 90.5% increase was observed.

The CV curves of Figure 6c show that the results of AC YSC after 1st cycle of exposure to the environment and the control are almost identical. The CV curves of Figure 6c are very close with insignificant differences. Unlike the resistance results of AC YSC in single-layer plain weave (Figure 6b), the resistance values of AC YSC in tubular structure (Figure 6d) increased after each exposure to the environment. Regardless of weave type,

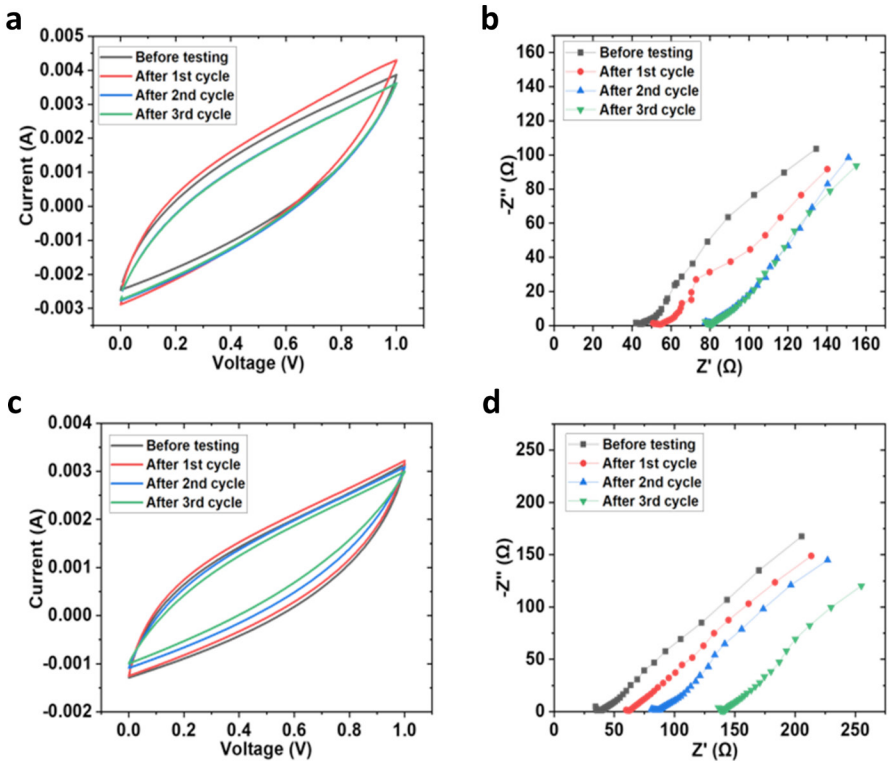

Figure 6: Electrochemical performance of AC YSCs of 45.72 cm long integrated in different woven fabrics upon exposure to environmental conditions. (a) CV curves (20 mV s^{-1}) and (b) Nyquist plots (1 M – 0.01 Hz) of AC YSCs in single-layer plain weave after each testing cycle; (c) CV curves (20 mV s^{-1}) and (d) Nyquist plots (1 M – 0.01 Hz) of AC YSCs in double-layer plain weave after each testing cycle.

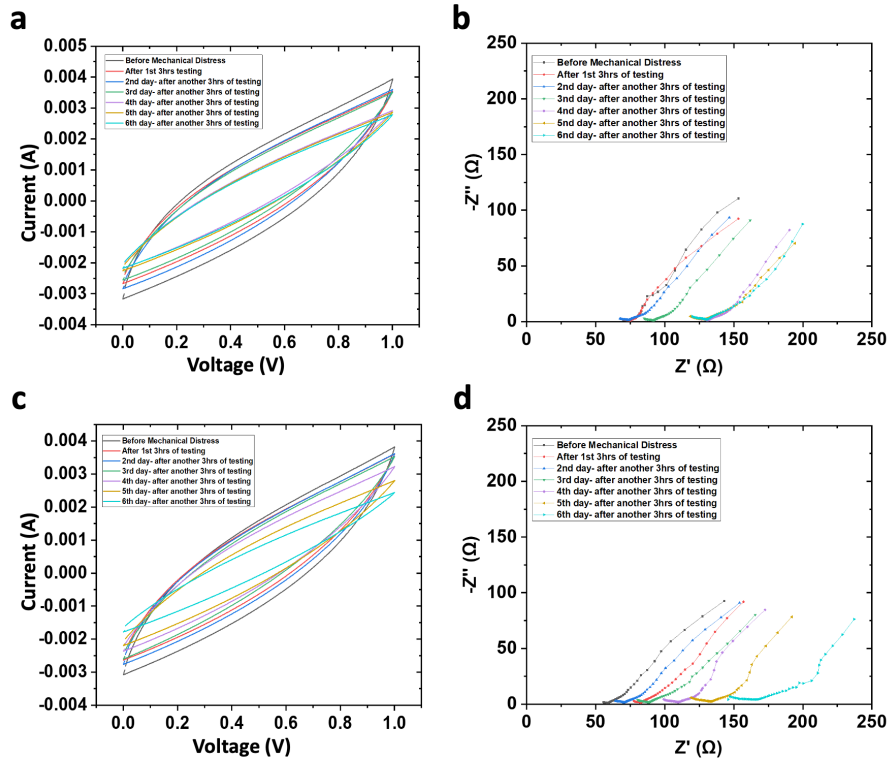

Figure 7: Electrochemical performance of AC YSCs of 45.72 cm long integrated in different woven fabrics upon accelerated mechanical distress. (a) CV curves (20 mV s^{-1}) and (b) Nyquist plots (1 M – 0.01 Hz) of AC YSCs in single-layer plain weave after each testing cycle; (c) CV curves (20 mV s^{-1}) and (d) Nyquist plots (1 M – 0.01 Hz) of AC YSCs in double-layer plain weave after each testing cycle.

the electrochemical performance of the AC YSCs did not change significantly compared to their control as a result of exposing the experimental samples to extreme hot/humid and cold environment. The single-layer plain weave and double-layer plain weave fabrics were exposed to the environment for long duration and hence the equilibrium reached equally to the AC YSCs regardless of the weave type. It is worth mentioning that the differences could be relevant to the variability in the formation of the YSCs processes.

Effect of Accelerated Distress Test

Figure 7 shows the electrochemical properties of the AC YSCs integrated in single-layer plain weave and double-layer plain weave samples. The results of CV of AC YSC in single-layer plain weave samples (Figure 7a) indicate degradation in AC YSC performance after the 4th cycle and the degradation after 5th and 6th cycles are identical. The resistance increased slightly after each cycle with a more noticeable increase after the 3rd cycle (Figure 7b), after which it remains relatively stable. This segmented degradation in both capacitance and resistance may be best explained by distress-induced yarn deformation in the single-layer case, which leads to inferior contact between the electrodes and gel electrolyte. After 3 cycles, this deformation tends to be permanent with litter further variation, which perhaps explains the overlapping CV and Nyquist plots for the 4~6 cycles. In the case of double-layer plain weave (Figure 7c and 7d) the results are comparable to those of single-layer plain weave with insignificant difference, except the factor that double weave again presented a more gradual and continuous increase in resistance upon cycles. We expected the "double-layer weave" to provide better protection for the YSCs upon distress, which is not evidenced in this set of experiments. The primary reason for this, as we perceive, is the relatively loose structure of YSCs inside the tubes of the double-layer sample, as compared to the rigid interlocking of YSCs in the single-layer plain-weave sample. The loose YSCs tend to be more continuously affected by repetitive distress cycles.

Effect of Abrasion Test

Figure 8 shows the electrochemical performance results of single-layer and double-layer plain weave samples with integrated AC YSCs after abrasion cycles using sandpaper abradant. The textile yarns of single-layer plain and the top layer of the double-layer plain weave samples failed before the AC YSCs performance deterioration at 1,200 cycles and 2,100 cycles, respectively. The CV data of the AC YSC (Figures 8a and 8c) integrated in single-layer and double-layer plain weave samples indicate a good performance despite the base fabric deterioration during the test. However, if the abrasion test continued, the AC YSC yarns will be torn after a few abrasion cycles. While the CV data for both AC YSCs in single-layer and double-layer fabric changed insignificantly, the CV data of AC YSC integrated in the tubes of

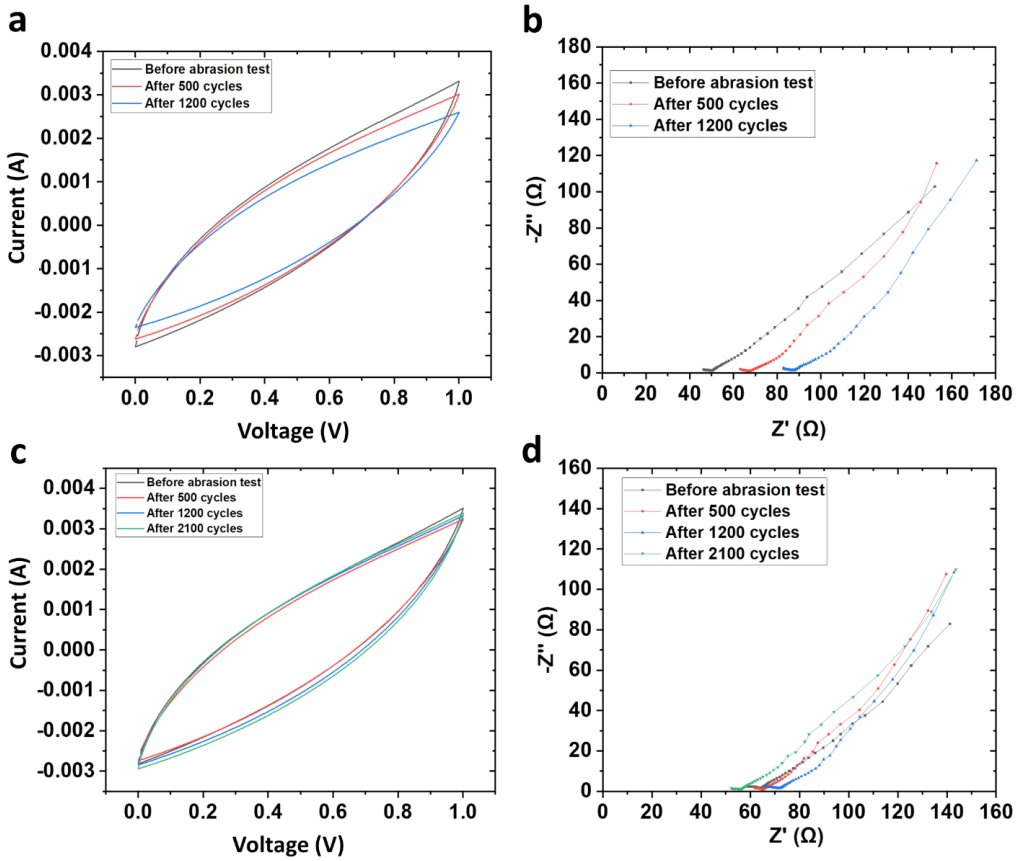

Figure 8: Electrochemical performance of AC YSCs of 45.72 cm long integrated in different woven fabrics upon abrasion against sandpaper. (a) CV curves (20 mV s^{-1}) and (b) Nyquist plots (1 M – 0.01 Hz) of AC YSCs in single-layer plain weave; (c) CV curves (20 mV s^{-1}) and (d) Nyquist plots (1 M – 0.01 Hz) of AC YSCs in double-layer plain weave.

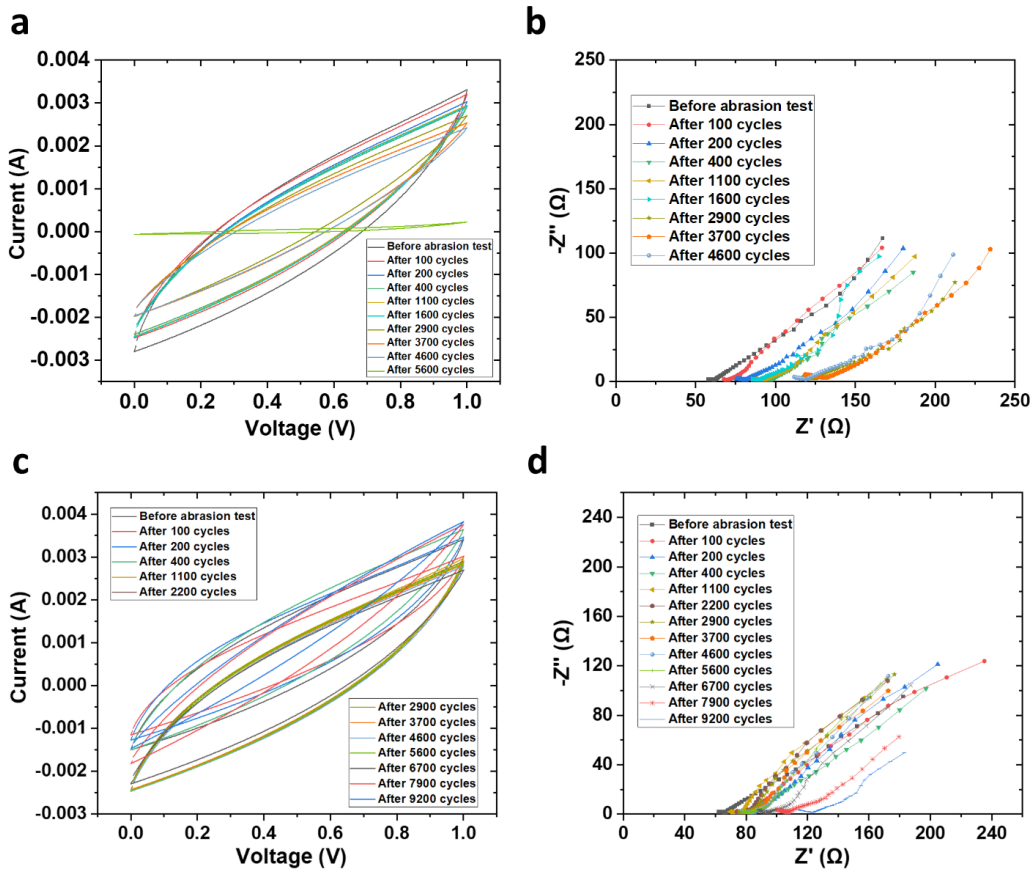

Figure 9: Electrochemical performance of AC YSCs of 45.72 cm long integrated in different woven fabrics upon abrasion against cotton duck. (a) CV curves (20 mV s^{-1}) and (b) Nyquist plots (1 M – 0.01 Hz) of AC YSCs in single-layer plain weave; (c) CV curves (20 mV s^{-1}) and (d) Nyquist plots (1 M – 0.01 Hz) of AC YSCs in double-layer plain weave.

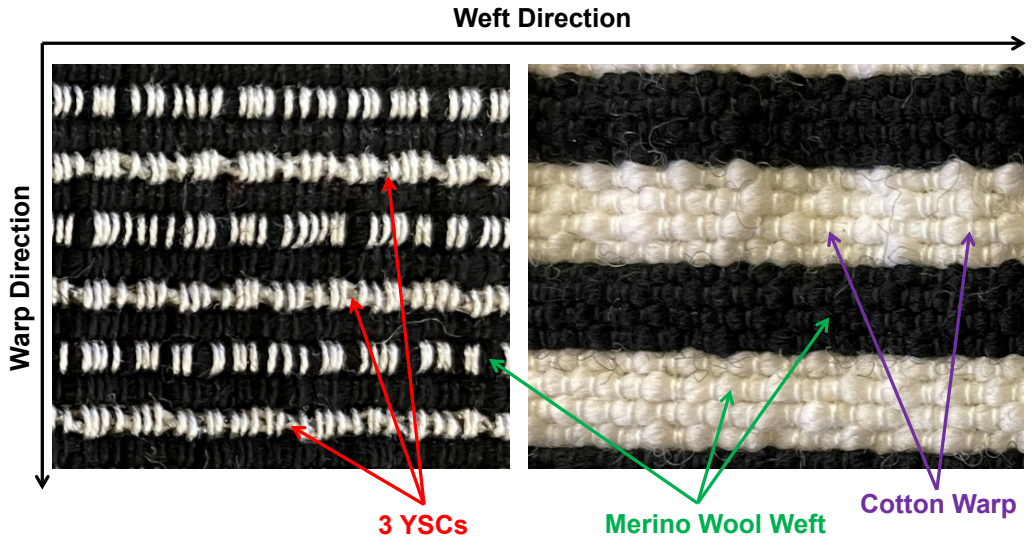

Figure 10: Photographic images of our single-layer (left) and double-layer (right) plain weave fabrics. 40/2 Ne combed, ring spun, mercerized cotton yarns were used as the warp yarns in both fabrics. On the left, the single-layer weave was made from black wool weft yarns with integrated AC YSCs every fourth weft, as indicated by red arrows in the figure. On the right, the double-layer plain weave fabric was made from white/black merino wool weft yarns (pointed out with the green arrows in the figure), alternatively placed to give us the white/black horizontal stripes, and the AC YSCs are incorporated between the top layer and bottom layer (invisible in the picture).

the double-layer sample are almost superimposed regardless of the number of abrasion cycles. Same observations are noticed for the resistance data of the AC YSC (Figures 8b and 8d). The increase in the internal resistance with abrasion cycles of AC YSC integrated in double-layer sample is lower than that of the AC YSC integrated in single-layer sample. The abrasion resistance of the double-layer sample is superior to the single-layer samples, and as such double-layer sample provides longer protection for the AC YSC. Previous work evaluated e-textiles of single-layer woven fabric [19,20].

Figure 9 shows the electrochemical performance of AC YSC integrated in single-layer and double-layer plain weave samples after abrasion cycles using standard #10 Cotton Duck abradant. As shown in Figure 9a & Figure 9b, the single-layer sample lost its electrochemical performance at the 5600th abrasion cycle. Though the double-layer sample presents a decline in performance after 5,600 abrasion cycles, it still maintained a certain level of performance up to 9,200 abrasion cycles (Figure 9c & Figure 9d). These results suggest that the double-layer plain weave samples provided better protection for the AC YSCs than the single-layer plain weave samples, as the AC YSCs are not in direct contact with the abradant. In contrast to sandpaper, Cotton Duck are much softer and compressible, therefore, both single-layer and double-layer plain weave samples demonstrate superior stability compared to those using sandpaper abradant.

As mentioned earlier, the single-layer and double layer plain woven fabrics were designed with careful selection of structural parameters to provide maximum protection and maintain the electrochemical integrity for the AC YSC from wear during end use. Figure 10 shows single-layer and double-layer plain weave fabrics before the abrasion test and their protective features for the AC YSCs. As the cotton warp yarns (black and white arranged in the vertical direction) crimp (31%) is the highest followed by the wool weft yarns (2.6%) (black in single-layer and white/black in double-layer arranged in the horizontal direction) and 0% crimp of the AC YSC, the crowns of the warp yarns are the most protruding out of the surface of the fabric followed by the crowns of the wool weft yarns while the AC YSCs do not exhibit crowns as they are lying flat with no crimp.

In single-layer fabric, during abrasion test, the warp yarns and wool weft yarns are in contact with the abradant throughout the test until failure while the AC YSC are not in contact with the abradant (i.e., the abradant must go through the textile yarns before contacting the AC YSCs). The warp yarns failed first, wool weft yarns failed partially as they partially share the surface of the fabric with the warp yarns. As the weft yarns are thicker with lower crimp than warp yarns, they fail next and hence the entire base fabric. This explanation is supported by observations as the test was stopped to measure the electrochemical performance of the AC YSCs.

The damage mechanism of the double-layer samples is the same in terms of sequence of yarns' failure. The reason why the top layer of the double-layer required more abrasion cycles to damage is the higher number of wool weft yarns woven in the top layer per AC YSC (4 in double-layer vs 3 in single-layer). An additional reason may be attributed to the tubular structure as the top layer may move while being abraded and partially avoid the abrasion energy from the abradant. Moreover, the bottom layer of the double-layer fabric provides cushion effect to the top layer as opposed to the solid head of the Wyzenbeek abrasion tester that applies pressure on the sample during testing that a single-layer experiences.

It is worth noting that the protective features of the woven structures not only provide shielding against abrasion but also against pressure and abrasion the fabrics are experiencing during weaving as they are wound under tension on the cloth roll by the fabric take-up mechanism, that contributed to maintaining the supercapacitor electrochemical integrity after weaving.

Conclusion

We have developed yarn-shaped supercapacitors (AC YSCs) with reasonable capacitance and ESR output, decent flexibility, and small-enough diameter to be compatible with automated weaving processes, which can be potential power sources for wearable textiles with rechargeability. The AC YSCs were directly integrated into different weave structures (single-layer and double-layer plain weaves) using computer controlled automatic shuttle weaving machine and their electrochemical performance, assessed by CV and Nyquist plots, was not negatively influenced by the rigor of the preparation prior weaving and during the weaving process, whether the AC YSCs were integrated in warp or weft direction.

The AC YSCs demonstrated resilience under extreme temperature conditions, enduring three days of both extremely hot and humid environment followed by extremely cold environment cycles. Additionally, all AC YSCs incorporating fabrics exhibited the capacity to withstand long duration of accelerated mechanical distress. These fabrics also present decent abrasion resistance when subjected to standard Cotton Duck abradant in Wyzenbeek abrasion test, however, proved susceptible to more abrasive conditions involving sandpaper abradant. Integrating the AC YSCs into the tubes of the double-layer plain weave structure provided better protection as it resulted in prolonged resistance to abrasion. Therefore, the adoption of a more robust and protective weave architecture using abrasion resistance textile fibers such as nylon and nylon blends is advisable to enhance the abrasion resistance of fabrics containing AC YSCs, particularly for fabrics exposed to intensive abrasion.

Future research endeavors should concentrate on both YSCs and fabric-level investigations. Further efforts can be focused on devising novel physical testing methods tailored to practical application contexts. In addition, the structure and composition of YSCs can also be optimized to enhance their electrochemical performance and textile properties (higher capacitance, lower resistance, smaller diameter, and higher flexibility). Furthermore, the design and implementation of woven structures that provide superior protection for YSCs merit attention. Strategical placement of the YSCs into wearable textiles to avoid high distress and friction could prolong their endurance during real-life applications.

References

1. Shi J, Liu S, Zhang L, et al. Smart Textile-Integrated Microelectronic Systems for Wearable Applications. Adv Mater. 2020; 32: 1901958.
2. Wang H, Zhang Y, Liang X, et al. Smart Fibers and Textiles for Personal Health Management. ACS Nano. 2021; 15: 12497-12508.
3. Libanori A, Chen G, Zhao X, et al. Smart Textiles for Personalized Healthcare. Nat Electron. 2022; 5: 142-156.
4. Choudhry NA, Arnold L, Rasheed A, et al. Textronics—A Review of Textile-Based Wearable Electronics. Advanced Engineering Materials. 2021; 23: 2100469.
5. Baeg KJ, Lee J. Flexible Electronic Systems on Plastic Substrates and Textiles for Smart Wearable Technologies. Advanced Materials Technologies. 2020; 5: 2000071.
6. Stanley J, Hunt JA, Kunovski P, et al. A Review of Connectors and Joining Technologies for Electronic Textiles. Engineering Reports. 2022; 4: e12491.
7. Ruckdashel RR, Venkataraman D, Park JH. Smart Textiles: A Toolkit to Fashion the Future. J Appl Phys. 2021; 129: 130903.
8. Zhai S, Karahan HE, Wang C, et al. 1D Supercapacitors for Emerging Electronics: Current Status and Future Directions. Adv Mater. 2020; 32: e1902387.
9. Zhou Y, Wang CH, Lu W, et al. Recent Advances in Fiber-Shaped Supercapacitors and Lithium-Ion Batteries. Adv Mater. 2020; 32: e1902779.
10. Gao J, Shang K, Ding Y, et al. Material and Configuration Design Strategies towards Flexible and Wearable Power Supply Devices: A Review. J Mater Chem A. 2021; 9: 8950-8965.
11. Liu L, Yu Y, Yan C, et al. Wearable Energy-Dense and Power-Dense Supercapacitor Yarns Enabled by Scalable Graphene–Metallic Textile Composite Electrodes. Nat Commun. 2015; 6: 7260.
12. Khudiyev T, Lee JT, Cox JR, et al. 100 m Long Thermally Drawn Supercapacitor Fibers with Applications to 3D Printing and Textiles. Advanced Materials. 2020; 32: 2004971.
13. He J, Lu C, Jiang H, et al. Scalable Production of High-Performing Woven Lithium-Ion Fibre Batteries. Nature. 2021; 597: 57-63.
14. Liao M, Wang C, Hong Y, et al. Industrial Scale Production of Fibre Batteries by a Solution-Extrusion Method. Nat Nanotechnol. 2022; 17: 372-377.
15. Maity S, Singha K, Singha M. Recent Developments in Rapier Weaving Machines in Textiles. American Journal of Systems Science. 2012; 1: 7-16.
16. Chen X. Characteristics of Cloth Formation in Weaving and Their Influence on Fabric Parameters. Textile Research Journal. 2005; 75: 281-287.
17. He N, Song J, Liao J, et al. Separator Threads in Yarn-Shaped Supercapacitors to Avoid Short-Circuiting upon Length. npj Flexible Electronics. 2022; 6: 1-8.
18. Joshi B. Formation of Woven Structures with Embedded Flexible Supercapacitor Yarns and Their Applications. North Carolina State University. 2021.
19. Seyam AFM, Bogan KM, Slade J. Evaluation of the Electrical Integrity of E-Textiles Subjected to Abrasion. Journal of Textile and Apparel, Technology and Management. 2019; 11.
20. Bogan K, Seyam AFM, Slade J. Evaluation of the Electrical Integrity of E-Textiles Subjected to Environmental Conditions. The Journal of the Textile Institute. 2018; 109: 393-409.